Composites Part B 175 (2019) 107136

Contents lists available at ScienceDirect

Composites Part B

journal homepage: www.elsevier.com/locate/compositesb

Tribological behavior of ultrasonic assisted double stir casted novel nano-composite material (AA7150-hBN) using Taguchi technique

Pagidi Madhukar [a,*], N. Selvaraj [a], C.S.P. Rao [b], Veeresh Kumar G.B. [c]

[a] Department of Mechanical Engineering, National Institute of Technology, Warangal, Telangana, India
[b] National Institute of Technology - Andhra Pradesh, Tadepalligudem, Andhra Pradesh, India
[c] Department of Mechanical Engineering, National Institute of Technology - Andhra Pradesh, Tadepalligudem, Andhra Pradesh, India

ARTICLE INFO

Keywords:
Al7150 alloy
Ultrasonication
Stir casting
Nanocomposites
Hardness
Tribological characteristics

ABSTRACT

A novel Al-7150 nanocomposite material was fabricated with various weight percentages of Hexagonal Boron Nitride from 0.5 to 2 wt% in steps of 0.5 wt% by liquid metallurgy route via ultrasonic assisted double stir casting method. The tribological properties were tested and carried out on pin-on-disc tribometer considering various input parameters like weight percentage of reinforcement, applied load, sliding distance and speed to study the tribological characterization. Taguchi technique using MiniTab 17 software was used to analyse the wear rate of nanocomposites. Different experiments were conducted using Taguchi technique and the regression equations were developed through Analysis of Variance (ANOVA) to investigate the influence of various test parameters such as applied load, sliding distance, sliding speed and the material parameter such as weight percentage of reinforcements. The applied load had the greatest influence on statistical and physical properties of nano-composites while, the sliding speed exercised its impact on the Coefficient of Friction (COF) of nanocomposite on dry sliding wear and also on the optimal parameters for less wear rate and low COF. The worn-out surface morphology of test specimens was investigated through Scanning Electron Microscope (SEM), Energy-Dispersive X-ray spectroscopy (EDX) system and correlated with the obtained results and conclusions were drawn.

1. Introduction

The majority of researchers aimed for designing lighter materials coupled with high strength to weight ratio, resistance to corrosion for automobile and aerospace applications. To meet this demand, researchers have shifted their focus from monolithic materials to high performance materials like Aluminum (Al) based composite materials owing to its properties like light weight, higher stability at heavier loads, resistance to wear, coupled with good corrosion resistance. The Al-Metal Matrix Composites (MMCs) are produced by various techniques such as squeeze casting, spray deposition, powder and liquid metallurgy route specifically via stir casting method [1]. The liquid casting route is a highly interesting technique due to its flexibility with economics in the fabrication of Al-MMCs [2]. Al-MMCs exhibit better mechanical properties with particulate (p) reinforcements because of its high strength and improved wear resistance than the unreinforced Al alloy [3]. From the recent past the Nanocomposites are attracting the attention of researches because they have low density, high strength and other properties such as high thermal conductivity, low Coefficient of Thermal Expansion (CTE) and dumping properties [4]. The production of nano-composites is a very difficult process and faces several hurdles like random distribution of reinforcement particles, poor wettability, porosity, clusters and agglomerations formation during the fabrication. An ultrasonic-assisted stir casting method may overcome the above-mentioned difficulties and also improve the uniform distribution of particles and wettability [5]. The double stir casting (compo casting) technique was adopted to improve the uniform distribution of nano-particles during the fabrication of Al-Metal Matrix Nano-Composites (MMNCs) [6]. In a study of Al-Graphene MMNCs, the nano-grains during the reheating process significantly enhanced the yield strength. The graphene sheets with onion shape have decreased the agglomeration of Silicon Carbide (SiC) nanoparticles. As a result of wrapping graphene sheets, resulted in lessening the porosity, thereby enhancing the tensile properties of the Al-MMNCs [7]. Shusen Wu et al., studied the microstructure and mechanical properties of nano-SiCp/Al MMNCs by diluting the molten Al under Ultrasonic Vibration (UV) via squeeze casting and noticed that the nano-SiCp are uniformly distributed in the Al-SiCp MMNCs and the tensile strength of the MMNCs improved

* Corresponding author.
E-mail address: pmadhu88@gmail.com (P. Madhukar).

https://doi.org/10.1016/j.compositesb.2019.107136
Received 29 November 2018; Received in revised form 19 June 2019; Accepted 5 July 2019
Available online 6 July 2019
1359-8368/

compared to Al356 alloy matrix [8]. In a study of γ- Aluminum Oxide (Al_2O_3)/A356 MMNCs the Ultimate Tensile Strength (UTS) and elongation of the MMNCs enhanced by 43.6% & 85.7% respectively and the improvement was attributed to the homogeneous distribution of the nanoparticles and refinement of the grains [9]. The Al-Cupper (Cu) MMNCs with Magnesium Silicide (Mg_2Si)-nanoSiCp subjected to microstructure and mechanical properties studies. The UTS and yield strength results indicated higher values than the other composites with good ductility. The improvement in the properties were attributed to the refined eutectic Mg_2Si phases in Mg_2Si-SiC/Al-Cu MMNCs [10]. The Al6005-Titanium Boride (TiB_2) MMNCs fabricated via Mechanical Alloying (MA) and hot extrusion was shown good distribution of the nano-reinforcement through optical studies and nano-indentation test shows an increment in hardness values with TiB_2 reinforcement in the Al6005 alloy [11]. Al6061-Zirconium Diboride (ZrB_2) MMNCs properties like hardness, strength and elongation were significantly improved due to the ZrB_2 nano-dispersoids and a quantitative calculation indicated that as ZrB_2 content increased, Orowan strengthening contributed to improved yield strength [12]. The P/M route developed Al-Boron Carbide (B_4C) MMNCs, showed that the hardness of the Al-B_4C MMNCs were higher than Al whereas the density and electrical conductivity of Al-B_4C MMNCs were lower than pure Al. This behavior has been explained by Hall–Petch Model and Orowan strengthening [13]. Al-Titanium Carbide (TiC) MMNCs synthesized by MA with nano-diamonds as precursors. The differential scanning calorimetry showed that the composite developed was stable within a wide range of temperatures, which permit its application in casting technologies [14]. Shimaa A et al., prepared Al/Ni-SiC MMNCs with nano-Ni and SiCp as reinforcements by P/M process and concluded that an enhancement in the CTE with increasing Ni-SiC percentage [15]. The Al6061-SiC-Graphite (Gr) hybrid MMNCs, the influence of nano SiC and Gr content resulted in improved wear resistance, lower COF and superior surface smoothness compared to Al6061 alloy [16]. In a microstructural study of Gr-B_4C hybrid reinforced ZA27 MMNCs fabricated via Mechanical Milling (MM) and hot pressing, the optical results revealed that MM method can be utilized for homogeneous distribution of the nano-sized additives in the matrix alloy [17]. Al6061 alloy was reinforced with Titanium Carbide (TiC), Al_2O_3 and hybrid (TiC + Al_2O_3) nanoparticles, the wear tests indicated that the wear rate increased with the load and sliding velocity. Hybrid Al6061 MMNCs had lower wear rate and COF compared with the other MMNCs investigated [18]. Beitallah Eghbali et al., fabricated the Al2024-Silicon Dioxide (SiO_2)-Titanium Dioxide (TiO_2) hybrid MMNCs, the structural and mechanical properties were examined and indicated an increase in the hardness, tensile and yield strength of hybrid MMNCs. The Al7075-SiC MMNCs fabricated through stir casting technique to provide significant benefits compared to other methods in terms of enhanced mechanical characteristics compared with unreinforced Al7075 [19]. In a study of P/M synthesized Cu-B_4C MMNCs on the microstructure and abrasive wear performance, the MMNCs with 1.5 wt% of B_4C revealed superior micro-hardness and wear resistance [20]. In a study of Graphene reinforced Cu matrix MMNCs optical studies confirmed even distribution of the reinforcement phase in the matrix with nano-crystalline microstructure and strong interfacial bonding between Cu and graphene with improved hardness and Young's modulus. The increment in strength was attributed to the microstructural refinement and dislocation pinning at the strong matrix-reinforcement interface [21]. The of dry sliding wear behavior of pure Magnesium (Mg) and Mg-MMNCs synthesized by P/M followed by hot extrusion process showed that the Mg-MMNCs wear level raises with higher sliding speeds and loads. Mg-MMNCs showed lower wear rates and COF compared with other MMNCs considered [22]. Jinling Liu et al., investigated the dry sliding wear behavior of Mg based MMNCs using ball-on-disk wear tester. Indicated that the COF of Mg-SiC MMNCs was much higher than pure Mg and suggested that the dominant wear mechanism was oxidation [23]. A model was developed to predict the wear rate by using regression model and Taguchi analysis for fabricated Al356-SiC MMNCs and the developed model predicted wear rate values were in close agreement with the experimental values [24]. Researchers across the globe have discovered that Al7XXX series of Al-Zn alloys meet desired properties and ideal for aerospace applications. The Lubricants are externally applied at contact surfaces to reduce the wear losses and specifically in periodic applications, lubricating is very difficult. For such applications, solid lubricants are preferred. Hexagonal Boron Nitride (hBN) is widely used as solid lubricant. Most of the Al alloys ware very soft and offer lesser resistance to wear. Therefore, to enhance the wear resistance the present investigation is aimed at the fabrication Al7150-hBN nanocomposites with improved hardness.

2. Experimental procedure

2.1. Materials

Al-7150 alloy was procured from Venuka Engineering Pvt Ltd., Hyderabad, India. The chemical composition of AA7150 is given in Table 1. The hBN nano-powder was obtained from Sisco Research laboratories Pvt Ltd., India. The average particle size of hBN was 70 nm. The coarser grain size Mg and solid degasser tablet Hexachloroethane (C_2Cl_6) are from Taranath Scientific & Chemical Company, Hanamkonda, India. Mg is used to improving wettability of nano particulates during the fabrication. Table 2 shows the properties of matrix and reinforcement materials.

2.2. Fabrication process

The Ultrasonic assisted stir casting is the most promising technique in liquid metallurgy for the production of MMNCs economically [25]. To improve the effectiveness of stir casting, two-step stirring was considered known as *Rheocasting or Double Stir Casting Technique* was adopted in the current studies for the fabrication. This process involves a total 20 min of stirring action in two steps. Each step has been carried-out for about 10 min, between the steps; the melt was allowed to cool down to semisolid state and then re-melted to perform the next step of stirring process to produce uniform distribution nano-particulates in the matrix. The Mg particles were added to the molten metal during stirring to improve the bonding between nanoparticles and matrix. Al7150 is melted to 750 °C and 500 °C pre-heated hBN nano-reinforcement particles were added into the vortex of the molten Al7150 after effective degassing with a solid degassing C_2Cl_6 tablet. After that ultrasonication process was done for about 10 min to obtain uniform distribution of particles in the molten matrix. The molten composite then poured into pre-heated mould box and allowed to solidify. The solidified cylindrical composites were removed from the mould and the specimens were machined as per ASTM standards for various testing. The Vicker's micro-hardness tester model: ECONOMET VH 1MD, was used to find the hardness of matrix and Al7150-hBN MMNCs at a load of 200 g with 15 s dwell time. The metallographic tests were conducted on the test samples with the help of SEM model: Vega 3 LMU model, Tescon make and respective elemental and chemical analysis was done with EDX model: Oxford Instruments, U.K.

2.3. Wear test

The counter disc of EN 31 hardened steel with a 62 HRC used for the current study in POD. The nanocomposite test samples were prepared as per ASTM G-99 standards with a dimensions of diameter 8 mm and

Table 1
The chemical composition of Al7150 alloy in weight percentage.

Element	Zn	Cu	Mg	Fe	Zr	Si	Mn	Al
AA7150	6.37	2.25	2.56	0.12	0.11	0.08	0.009	Balance

Table 2
Material properties of Al7150 alloy and hBN.

Materials	Modulus of Elastic (GPa)	Density (g/cc)	Hardness (HV)	Tensile Strength (MPa)
Al7150	70	2.83	41	140
hBN	675	2.21	194	620

30 mm in length specimens. All the samples were polished using different grades to maintain flatness for the wear test so as to establish proper contact with the counter disc. The pin and disc surface roughness of 0.1 μm Ra were maintained and at the end of each test, the disc surface was cleaned by acetone. The experimental set-up is as shown in Fig. 1.

The wear test experiment is designed to elevate two or more factors, which are able to affect the output parameters such as wear rate and COF for the particular product. The complete results of the test combination are observed and analyzed to find the particular level of factors affecting wear parameters. Taguchi's method is the most prominent optimization tool for solving typical design problems. In comparison with the full factorial design problems, Taguchi's technique will reduce the number of experiments that are required to model the responses, further, it will optimize the parameters which are affecting the wear of the materials.

2.4. Plan of experiments

The wear tests were planned for Al7150-hBN MMNCs samples were subjected to dry sliding tests for 4 factors such as Sliding Distance (SD) in meters, Sliding Speed (SV) in m/sec, Applied Load in Newtons (N) and Percentage of Weight (wt%) of reinforcement for 5 levels as shown in Table 3.

The experiments were planned according to L25 orthogonal array standard as shown in Table 4 and were assigned sliding distance (SD), sliding speed (SV), applied load (L) and percentage weight (%wt) of reinforcement of nanoparticles at various values. The current investigation is based on the output parameters such as Wear Rate (WR), COF, temperature to study *"smaller is the best"* responses.

3. Results and discussion

3.1. Elemental analysis

The fabricated Al7150-hBN MMNCs with 0.5–2 wt% in steps of 0.5 wt% by liquid metallurgy route via ultrasonic assisted double stir casting method were subjected to the metallographic studies via SEM and EDX analysis. The obtained SEM images along with the with EDX elemental analysis are mentioned and discussed in this section.

From the metallographic studies, it is observed that the hBN nanoparticles in the Al7150 alloy and dispersed evenly in the throughout the Al7150-hBN MMNCs. The Al alloy is highly influenced by 1 wt% Mg in the liquid metal for excellent bonding as well as homogeneous distribution of the nanoparticle throughout the composite in the casting process along with the ultrasonication. But the formation of small agglomerations and clusters are noticed with increase in wt% of reinforcements [26,27]. Further, it can be observed that there are a lot of agglomerations and clusters at 2 wt% of hBN in MMNCs (see Fig. 2).

3.2. Hardness of Al7150-hBN MMNCs

The Vicker's micro-hardness tester model: ECONOMET VH 1MD, was used to find the hardness of matrix and Al7150-hBN MMNCs at a load of 200 g with 15 s dwell time. The resistance to indentation tests were conducted in accordance with the ASTM E92 standards at room temperature. The Al7150 alloy and Al7150-hBN MMNCs hardness test results were presented and discussed in this section, each value of the hardness is an average of 5 measurements and the average hardness values of samples are represented through a bar chat as shown in Fig. 3.

From the figure it is evident that as the hBN content increases in the matrix alloy, there is a significant increase in the hardness of the MMNCs. The MMNCs containing 1.5 wt% hBN reinforcement material has highest micro-hardness in the current study. The amount of increase in hardness was 15% with the increase in the wt.% of hBN particulates from 0 to 1.5 wt% and at 2%hBN, the hardness decreases due to the formation of clusters during the mixing [28]. The increase in micro-hardness of Al7150-hBN MMNCs is mainly attributed to the fact that there is effective decrease in the grain size, good bonding between the matrix and reinforcement materials, due to this effective load transfer between Al7150 onto the hBN nano-particulates there is an increase in the hardness [29].

The hardness of nanocomposite increases with increase of hBN nanoparticles due to hard phase ceramic particles hBN and uniform distribution hBN nanoparticles which reduces the distance of interparticle with increasing of nanoparticle wt.% in the alloy matrix results in increase of resistance to indentation [30]. For the afforded hBN wt.% the nanoparticles are near to each other in the matrix and hence, ceramic nanoparticles will protest penetration of the indentation in the alloy matrix. The main strengthening mechanisms were estimated by Hall-Petch strengthening, Orowan strengthening, CTE mismatch and elastic modulus mismatch between the reinforcements and metal matrix. There was also some evidence showing some of the singular and agglomerated nanoparticles in the matrix of the nanocomposites [31].

3.3. Wear behavior

The wear experiments were conducted under dry-sliding condition as per ASTM G-99 standards at room temperature and the results are tabulated as shown in Table 5.

The influence of various factors has been considered such as load, sliding speed, sliding distance and wt.% of reinforcement particles, effect on COF, wear rate and temperature rise were evaluated using Signal to Noise (S/N) ratio [32]. The response analysis was carried-out for better understanding. Analysis of Variance (ANOVA) is used to develop

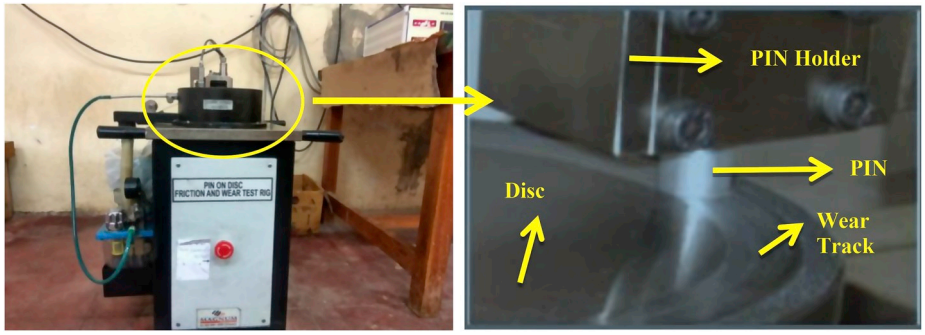

Fig. 1. Pin on dis experimental setup for a wear test.

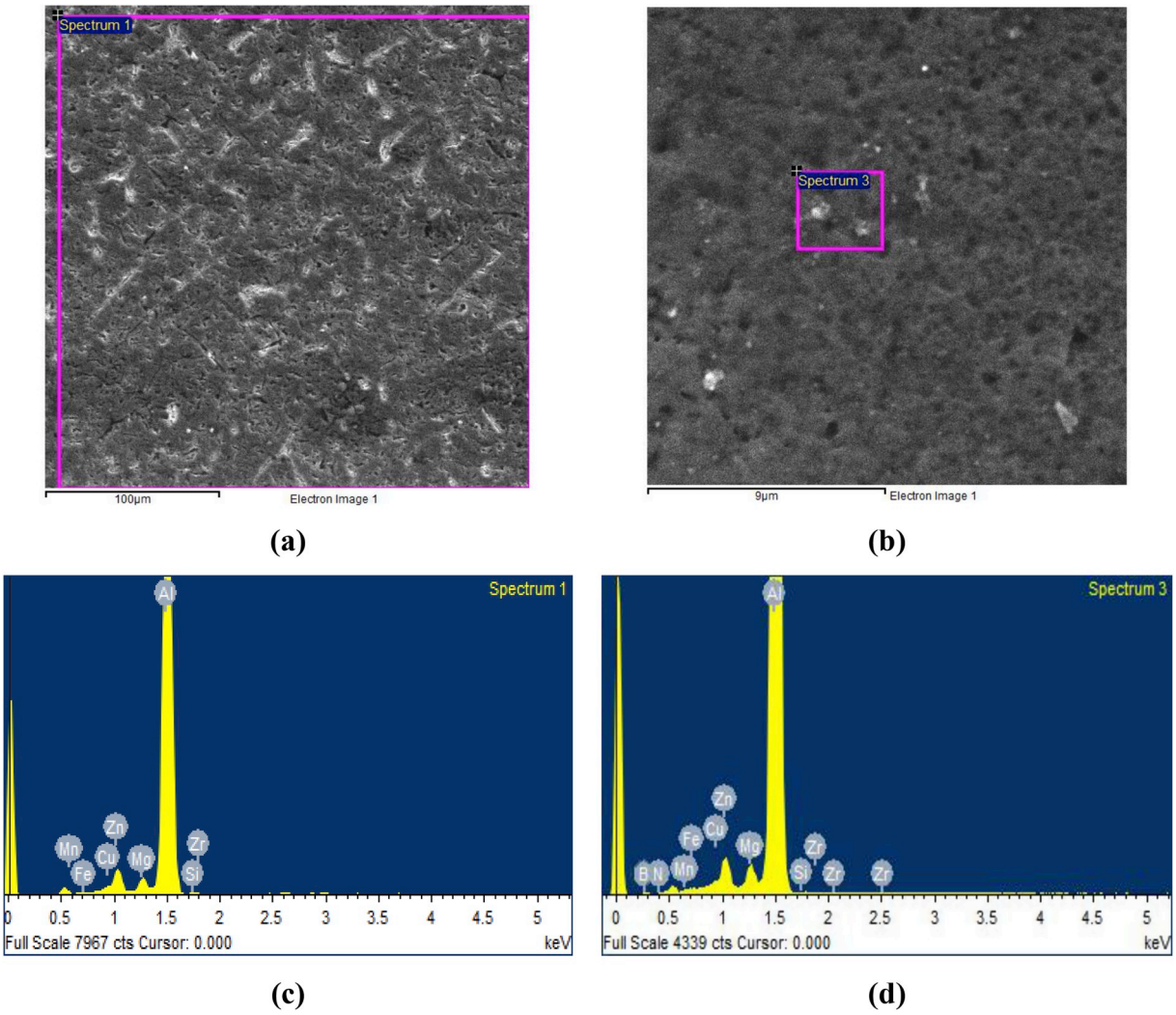

Fig. 2. SEM images (a) Al7150 alloy (b) Al7150–1.5 wt% hBN and EDS spectrum of (c) Al7150 alloy (d) Al7150–1.5 wt% hBN.

Table 3
Parameters are used in the experimentation.

Level	Wt %	Distance (m)	Speed (m/s)	Load (N)
1	0	500	0.5	10
2	0.5	1000	1.0	20
3	1.0	1500	1.5	30
4	1.5	2000	2.0	40
5	2.0	2500	2.5	50

the model and analyze the parameters and their interactions. The order of influence and the effect of parameters are studied on wear behavior using Minitab-17 software which is used in DOE applications.

The strongest influence of controlled parameters is identified by the maximum (max) and minimum (min) values difference of S/N ratio. The highest difference between the S/N ratio gives more influence of the control parameter. From these influencing parameters and output responses, such as wear rate, COF and temperature at the contact surfaces, better and smaller S/N ratio can be selected from the analysis. Therefore, the influencing parameters thus choosen are expected to improve material performance. Tables 6–8 show that the applied load is the most significant parameter among all other factors such as sliding distance, sliding speed and the weight percentage of reinforcements in case of wear rate as well as sliding speed for the COF and rise in the temperature of two mating parts. The graphical method suggests analyzing S/N ratio

Table 4
Taguchi method orthogonal array for L25.

S.No.	Wt%	Sliding Distance (m)	Sliding Velocity (m/s)	Load (N)
1	0	500	0.5	10
2	0	1000	1	20
3	0	1500	1.5	30
4	0	2000	2	40
5	0	2500	2.5	50
6	0.5	500	1	30
7	0.5	1000	1.5	40
8	0.5	1500	2	50
9	0.5	2000	2.5	10
10	0.5	2500	0.5	20
11	1	500	1.5	50
12	1	1000	2	10
13	1	1500	2.5	20
14	1	2000	0.5	30
15	1	2500	1	40
16	1.5	500	2	20
17	1.5	1000	2.5	30
18	1.5	1500	0.5	40
19	1.5	2000	1	50
20	1.5	2500	1.5	10
21	2	500	2.5	40
22	2	1000	0.5	50
23	2	1500	1	10
24	2	2000	1.5	20
25	2	2500	2	30

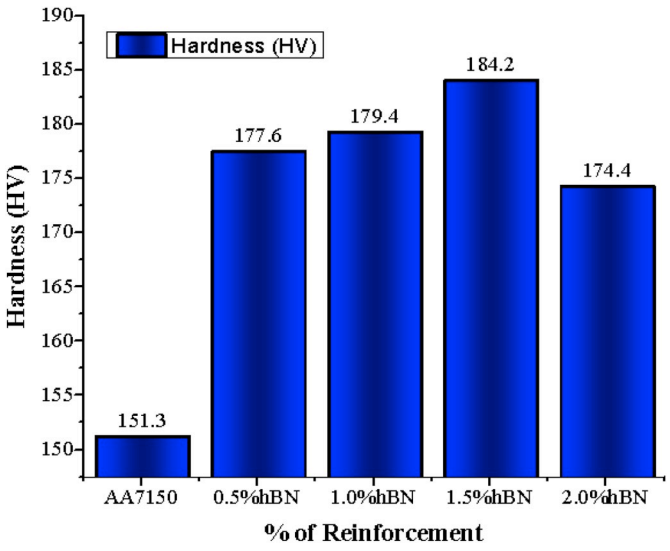

Fig. 3. Hardness values graphs for monolithic and MMNCs.

using a conceptual approach in Taguchi technique. The graphical representation of influencing parameters against the wear rate, COF and temperature rise at the contact of the surface is shown in Figs. 4–9.

The experiment was performed as per L25 Orthogonal array (Table 5 represented with the experimental details) and the results are tabulated in terms of WR, COF and Temperature rise (T) along with the S/N ratio values as shown in Table 5. The statistical values of parameters which exercise an impact on WR, COF and temperature rise are presented in main effects plots as shown in Figs. 4, 6 and 8 respectively.

From Fig. 4, it is clear that each parameter is different from others in influencing wear rate. For example, the lowest wear rate is seen when the wt.% of reinforcement is highest, i.e, the fifth level (2.0% hBN); at the same time, the same trend is followed in the sliding distance at fourth level (2000 m), whereas the same was realized when the sliding speed and load are the lowest, that is at the first level of graphical representation (0.5 m/s and 10 N).

According to Figs. 4, 6 and 8, an increase in wt.% of reinforcement particles results in hardness and strength of the MMNCs being high [33, 34], there is decreases in the wear rate, decrease in COF and rise in temperature due to the formation of solid lubrication layers from weak Van-der-Waal forces intern layers of hBN. These layers prevent higher wear rate and decrease COF on the pin surface [35]. This layer also acts as an insulating film to stop the heat transformation from the contact surface to pin material [36], while increasing the wt.% of reinforcement particles, the thickness of the solid lubricant layer also increases [37], resulting in lower wear rate, while the COF and temperature reduce [38]. Inclusion of wt.% of reinforcement also affects other parameters like sliding distance. As the sliding distance increases, the wear rate decreases [39] due to the solid lubricant effect between the contact surfaces, pin and disc materials upto certain limit. This lubricating film acts as an insulator and does not allow any rise in temperature to soften the pin material to undergo further wear.

In case of sliding speed and applied load, as the load increases, it increases the wear rate, COF and temperature [40,41]. The trend is shown in Figs. 4, 6 and 8. When the load is low, oxides form on the surfaces of the composites and interact with the metal contacting surfaces. These oxides significantly affect the tribo characteristics, resulting in lower COF and wear rate. Further, when the applied load is increased, the heat at contacting surface is also increased and this wear out the oxide layers, make the layers incapable of preventing the formation of additional layers at metallic contact surfaces, this frictional heat softens the pin material, resulting in enhancement in the grain size. This can be attributed to increase in contact surface area, the wear rate and further change to delamination with further increase of load [42–45] and the same trend can be observed in Figs. 6 and 8 which show increase in COF and temperature rise of the material.

Table 6
Analysis of Variance for wear rate (mm^3/m).

Source	DF	Seq SS	Adj SS	Adj MS	F	P	Pr(%)
Wt.%	4	1.407	1.407	0.3518	0.43	0.784	2.205
SD (m)	4	9.828	9.828	2.4569	3.00	0.087	15.402
SV (m/s)	4	11.333	11.333	2.8332	3.45	0.064	17.761
Load (N)	4	34.677	34.677	8.6692	10.57	0.003	54.346
RE[a]	8	6.563	6.563	0.8203			10.285
Total	24	63.807					

[a] Residual Error.

Table 5
Wear test results as per L25 orthogonal array.

S.No.	Wt%	SD (m)	SV (m/s)	Load (N)	Wear rate (mm^3/m)*10^{-5}	S/N ratio for wear	COF	S/N ratio for COF	Temp (^oC)	S/N ratio for Temp
1	0	500	0.5	10	1.4947	−3.4911	0.48315	6.3184	36	−31.1261
2	0	1000	1	20	4.7781	−13.5851	0.4553	6.834	39	−31.8213
3	0	1500	1.5	30	3.4971	−10.8742	0.3653	8.7472	45	−33.0643
4	0	2000	2	40	5.0777	−14.1133	0.3596	8.8836	60	−35.563
5	0	2500	2.5	50	5.1837	−14.2928	0.28751	10.827	66	−36.3909
6	0.5	500	1	30	5.1416	−14.222	0.4642	6.6659	42	−32.465
7	0.5	1000	1.5	40	4.9292	−13.8555	0.3071	10.2544	48	−33.6248
8	0.5	1500	2	50	6.9617	−16.8543	0.3485	9.1559	67	−36.5215
9	0.5	2000	2.5	10	1.5221	−3.6489	0.22022	13.143	45	−33.0643
10	0.5	2500	0.5	20	1.4584	−3.2775	0.50455	5.9419	38	−31.5957
11	1	500	1.5	50	6.5007	−16.2592	0.42026	7.5297	52	−34.3201
12	1	1000	2	10	2.5631	−8.1753	0.2659	11.5056	45	−33.0643
13	1	1500	2.5	20	3.9537	−11.9401	0.23805	12.4666	53	−34.4855
14	1	2000	0.5	30	1.6489	−4.3439	0.51235	5.8087	39	−31.8213
15	1	2500	1	40	3.5603	−11.0297	0.48512	6.2829	46	−33.2552
16	1.5	500	2	20	3.6419	−11.2266	0.2748	11.2197	44	−32.8691
17	1.5	1000	2.5	30	4.6643	−13.3757	0.24025	12.3866	54	−34.6479
18	1.5	1500	0.5	40	2.9815	−9.4887	0.5235	5.6217	40	−32.0412
19	1.5	2000	1	50	4.0702	−12.1923	0.4945	6.1167	47	−33.442
20	1.5	2500	1.5	10	2.7904	−8.9133	0.33515	9.4952	44	−32.8691
21	2	500	2.5	40	5.974	−15.5253	0.25041	12.0269	54	−34.6479
22	2	1000	0.5	50	4.5285	−13.1191	0.53125	5.494	42	−32.465
23	2	1500	1	10	1.4437	−3.1895	0.4119	7.7042	42	−32.465
24	2	2000	1.5	20	2.6655	−8.5156	0.34531	9.2359	48	−33.6248
25	2	2500	2	30	2.3523	−7.4299	0.3162	10.0008	57	−35.1175

Table 7
Analysis of Variance for the coefficient of friction.

Source	DF	Seq SS	Adj SS	Adj MS	F	P	Pr%
Wt.%	4	0.001689	0.001689	0.000422	0.93	0.491	0.6
SD (m)	4	0.002276	0.002276	0.000569	1.26	0.362	0.89
SV (m/s)	4	0.233125	0.233125	0.058281	128.71	0.000	91.27
Load (N)	4	0.014709	0.014709	0.003677	8.12	0.006	5.76
RE	8	0.003622	0.003622	0.000453			1.418
Total	24	0.255422					

Table 8
Analysis of Variance for Temperature rise.

Source	DF	Seq SS	Adj SS	Adj MS	F	P	Pr%
Wt.%	4	36.24	36.24	9.060	0.56	0.697	2.17
SD (m)	4	89.84	89.84	22.460	1.39	0.319	5.402
SV (m/s)	4	942.64	942.64	235.660	14.63	0.001	56.68
Load (N)	4	465.44	465.44	116.360	7.22	0.009	27.98
RE	8	128.88	128.88	16.110			7.749
Total	24	1663.04					

As seen from Fig. 6, each factor shows a different pattern from other in influencing the COF. For example, the lowest COF is seen, when the wt.% of reinforcement is highest (2.0% hBN). At the same time, the sliding speed is at fifth level (2.5 m/s), whereas the same is realized when the sliding distance and load are at second level (1000 m) and at first level (10 N), when the sliding speed increases, the temperature also rises [46,47] due to friction at the contact surfaces of the pin and disc material. This temperature at lower speed is able to soften the subsurface of the composite material and any further increase in speed, leads to a molten layer and the solid lubricant effect will also affect the pin material, causing it to skid. With this combined effect, the COF reduces with increase in sliding speed [48]. Fig. 8, shows the different curve patterns with various factors. The sliding speed, sliding distance and applied load show the same trend in the graphical representation of temperature. As these factors increase, the temperature of the pin material at the contact surface also increases due to frictional effect.

From Figs. 4, 6 and 8, the influencing factors are easy to identify at optimal positions. The values obtained in terms of the level of influencing factors, which induce the lowest COF, wear rate and temperature rise in the nanocomposite material are optimum ones. To attain the accuracy of experimental results, the S/N ratios are calculated for all the parameters and the results are depicted in Figs. 5, 7 and 9. The factor level at which the COF, WR and temperature are lowest is attained at the highest S/N ratio and this can be proved for all the parameters in Figs. 5, 7 and 9.

From the graphs for S/N ratio, the fifth level of wt.% of reinforcement, the fourth level of sliding distance, the first level of both sliding speed and applied load can be considered as optimal points for lower wear rate. Whereas COF is concerned, the optimal points for lower COF is at the fifth level of both wt.% of reinforcement and sliding speed, the second level of sliding distance and the first level of load. From the temperature graph, the optimal point for lower temperature rise at the fourth level of wt.% of reinforcement particles, the first level of other three parameters such as sliding distance, sliding speed and applied load can be observed.

The optimal solution of an orthogonal experiment will not appear in the design of experiment because on orthogonal array of experiments provides the same results that of full factorial design which reduces human efforts and valuable time during the experimentation. The optimal parameters can be obtained from the main effective plots and the experiments has to be separately tested for optimum response [49].

Wear resistance of Al7150-hBN MMNCs increase significantly (up to 1.5 wt% hBN) due to micro hardness enhancement and strengthening mechanism. The wear loss will increase with increase in applied load and wear resistance increases with increased wt.% of hBN, by layer formation due to hBN solid-lubricant property.

As per dry sliding wear concern at the applications of stringers, upper and lower wings of aircraft, floor breams, seat tracks, fuselage of an aircraft. The wear resistance plays a crucial role in relative movement at contact surfaces. Hence, 1.5 wt% hBN providing the max wear resistance

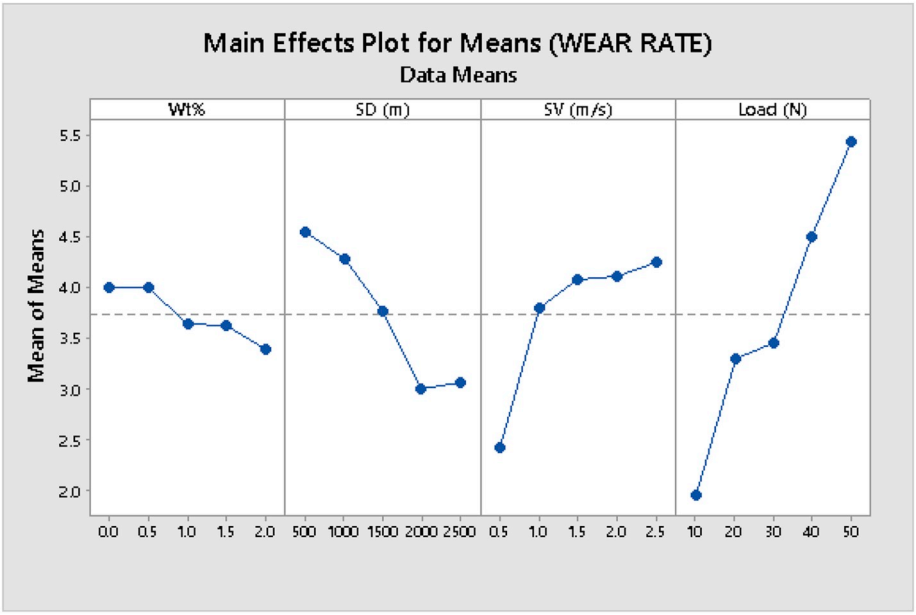

Fig. 4. Main effects plot for wear rate.

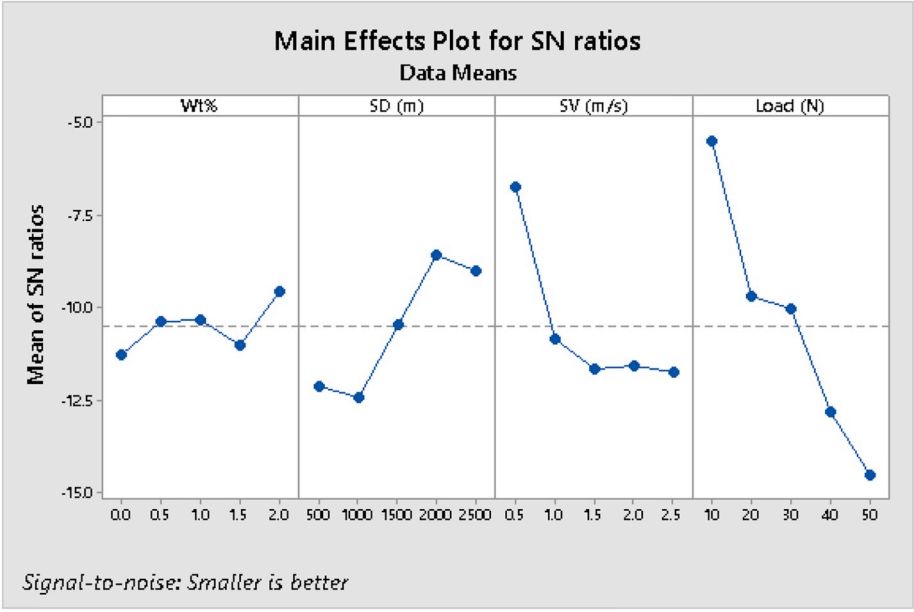

Fig. 5. WR Main effects plot for SN ratio.

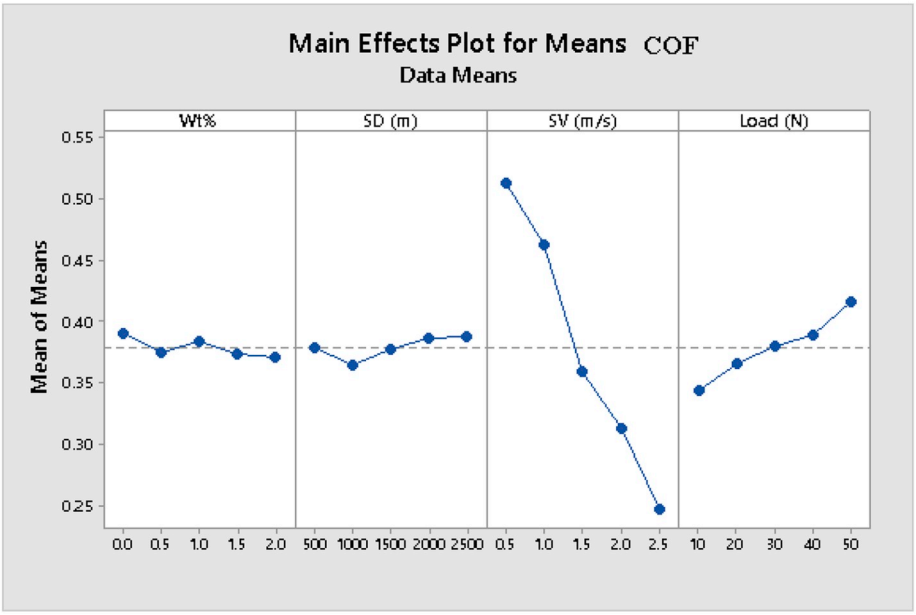

Fig. 6. Main effects plot for COF.

and strength to weight ratio for aerospace applications [50] in such cases 1.5 wt% hBN shows the better properties even for more applied load due to enhanced micro hardness.

The normal probability means plots for the experiment data have been done for the normality. The residual normal probability plots of COF, wear rate and temperature for hBN MMNCs are shown in Fig. 10a–c, which reveal that the falling residuals are on the straight line. This plots clearly indicate that the values of the responses lie very close to the normal probability line, signifying that the error is distributed normally. The graphs are plotted between the run order and residuals to test the independence of the experimental data for the COF, wear rate and temperature, and it confirms that there is no predictable pattern for all three responses. ANOVA technique is used for the significance of the experiment. The goodness of the model fit indicates R^2 for the formulated model for the COF, wear rate and temperature are represented by equations (1)–(3) respectively.

Fig. 11 shows the SEM images and EDX analysis of monolithic at min at 500 m SD, 0.5 m/s SV, 10 N L and max at 2500 m SD, 2.5 m/s SV, 50 N L conditions and for nanocomposite with 1 and 2 wt% of hBN worn surfaces. When the monolithic and nanocomposite materials come in contact with the counter surface, abrasion take place between asperities. The worn surface EDX profile of nanocomposite at AA7150 min and max conditions, AA7150-1 wt% and AA7150-2 wt% of hBN are as shown in Fig. 11 and the Aluminum predominant peaks, other chemical compositions, reinforcements with oxide (O) and iron (Fe) are observed. Fe peaks indicate the counter surface of steel disc material. The O peaks indicate the oxidation on worn surface due to high temperature at the contact surface and it is confirmed that the oxide layer act as a protective layer on the wear surface.

From the EDX profiles, the presence of O peak conforms to the

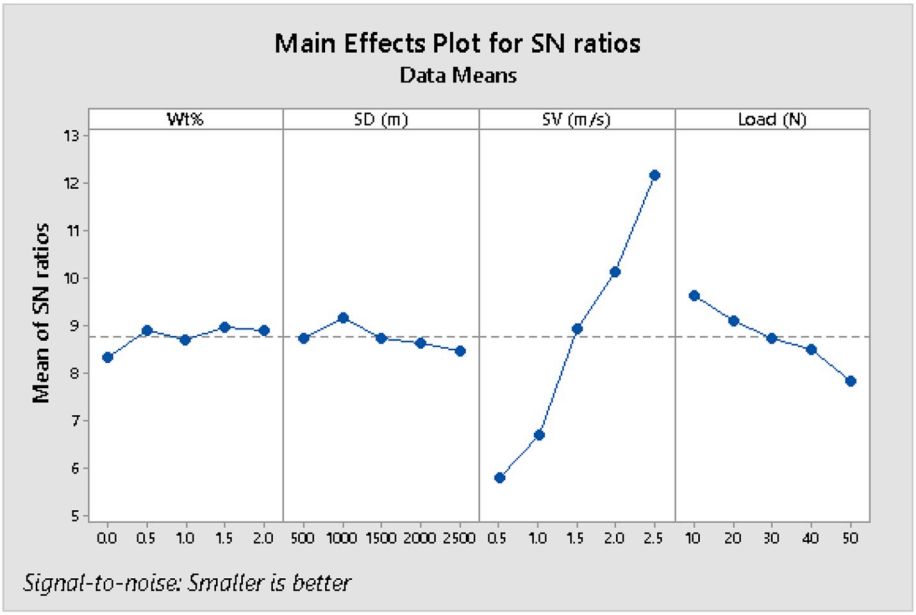

Fig. 7. COF Main effects plot for SN ratio.

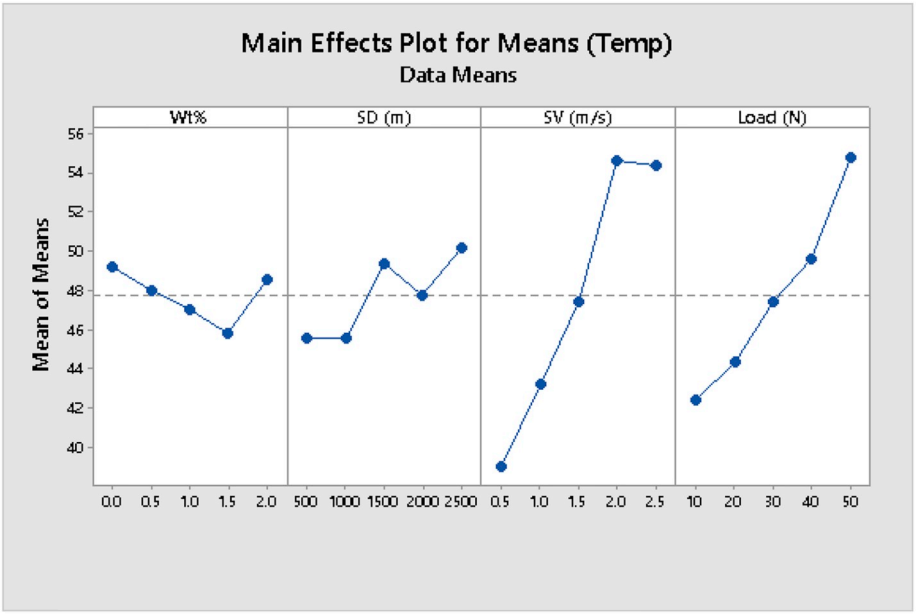

Fig. 8. Main effects plot for temperature.

oxidation wear [51]. In AA7150 wear, the presence of O peak is more at min condition as compared to max condition due to its low speed, which results in more oxidation. Fe peak is low at min condition as compared to max condition due to its high speed and load. The oxide percentage is less in 1 wt% hBN nanocomposite as compared to 2 wt% EDX spectrum due to more wt.% of hBN present and Fe is slightly varied due to solid lubricant property of hBN [52].

The final column of Tables 6–8 shows the ANOVA results of wear rate in mm^3/m, COF and temperature rise in °C for the materials considered. Table 6, shows the applied load (54.35%) had the greatest influence on nanocomposites while the sliding speed (17.76%) and distance (15.40%), wt.% (2.20%) did not have same influence on nanocomposites. It can also be observed that the interactions of SD*Load (2.44%), wt.% × Load (2.37%) are negligible because of low contribution and other interactions such as wt.% × SD, SD × SV, Wt.% × SV, SV × Load were 0.05–0.6% between and thus the influence was not comparable.

Table 7 shows that sliding speed (91.27%) had the greatest influence on nanocomposites, while the applied load (5.76%), sliding distance (0.89%) and wt.% of reinforcement (0.6%) were not as much influencing factors on the COF of nanocomposites. As for interactions, all interactions showed 0.001–0.15% contribution, therefore, the influence of these interaction factors do not allow of comparison.

As seen in Table 8, siding speed (56.68%) had the greatest influence on nanocomposites, while the applied load (27.98%), sliding distance (5.402%), wt.% of reinforcement particles (2.18%) did not show noticeable effect on the temperature increase in nanocomposites. The interactions wt.% × Load (3.95%) and SV × Load (3.11%) had a negligible influence and other combinations of interactions showed 0.02–1.7%; therefore, the influence these interactions factors are

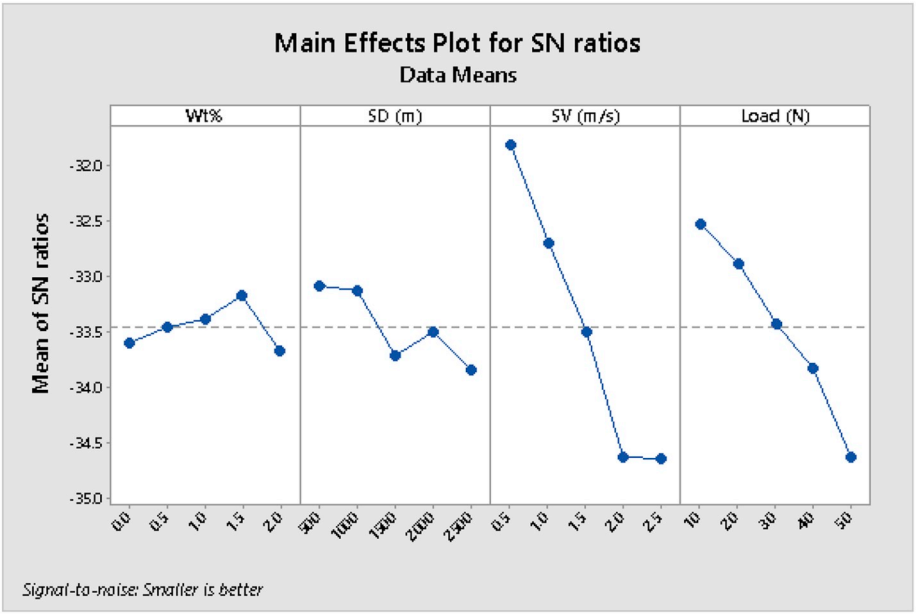

Fig. 9. Temp Main effects plot for SN ratio.

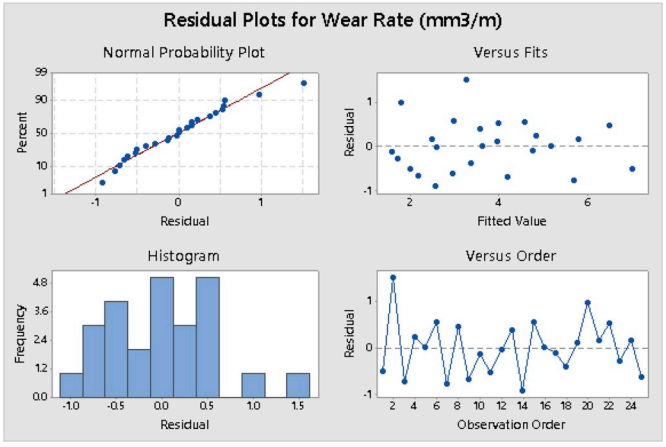

(a)

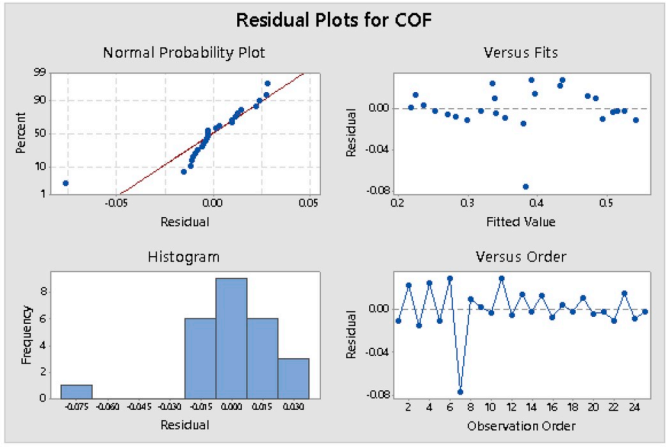

(b)

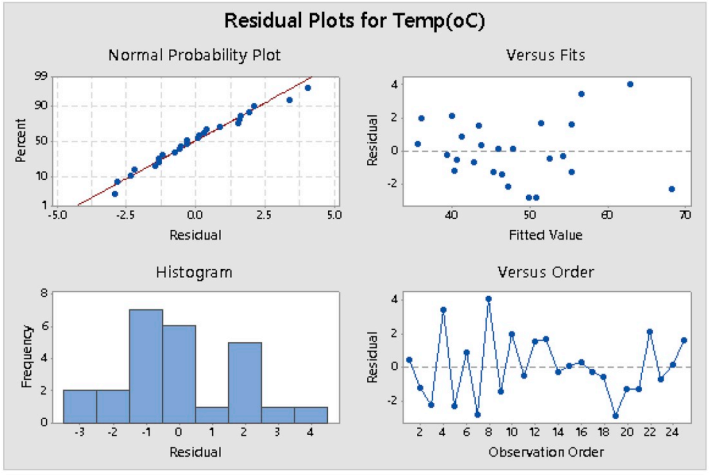

(c)

Fig. 10. Residual plots (a) Wear rate (b) COF (c) Temperature rise.

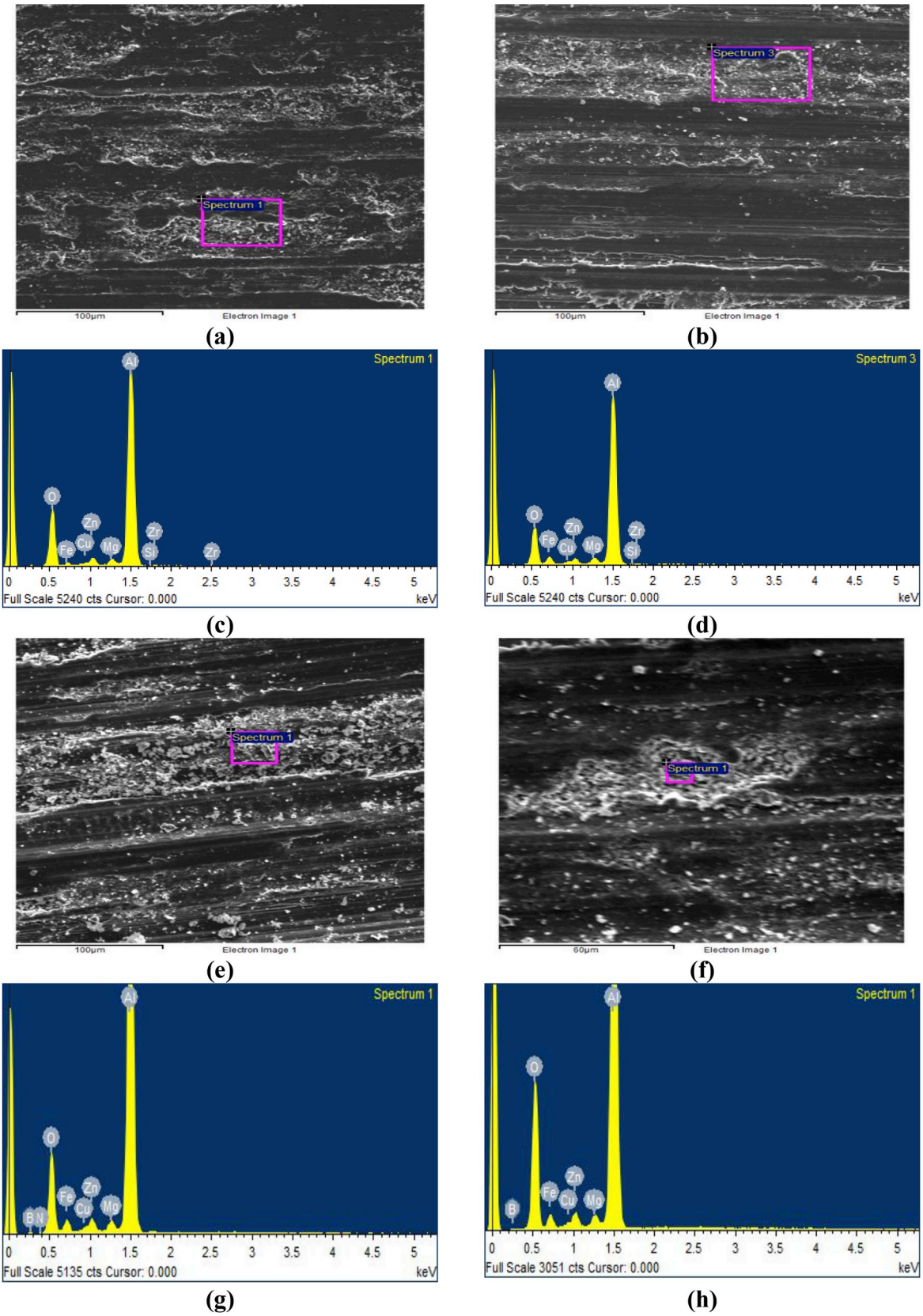

Fig. 11. SEM images and EDX patterns of (a) SEM image of Al7150 at min condition (b) EDX pattern at min condition (c) SEM image of Al7150 at max condition (d) EDX pattern at min condition (e) SEM image of 1 wt% hBN (f) SEM image of 2 wt% hBN (g) EDX pattern of 1 wt% hBN (h) EDX pattern of 2 wt% hBN nanocomposites after wear test.

incomparable. *'Smaller is the better'* for Wear rate Responses for the S/N ratios, COF Responses for the S/N ratios and Temperature Responses for S/N ratios are presented in the Tables 9–11.

4. Regression analysis

Minitab 17 software was used to correlate the wear factors such as sliding distance, sliding speed, applied load and the wt.% of nano-particles with the output responses such as WR, COF and Temperature under dry-sliding conditions. There are many regression models available. Among them, linear regression model was employed for tribological studies and it was found to have produced satisfactory results. Regression equations are developed for the COF, wear rate and temperature. The generated regression equations are as follows.

$$\begin{aligned} &Wear\ Rate = 0.44 - 0.469\ wt\% - 0.000172\ SD + 1.14\ SV + 0.124L \\ &R - square\ value\ = 87.15\% \end{aligned} \quad (1)$$

$$\begin{aligned} &COF = 0.5623 - 0.0144\ wt\% - 0.000002\ SD - 0.1571\ SV + 0.00072L \\ &R - square\ value\ = 96.06\% \end{aligned} \quad (2)$$

$$\begin{aligned} &Temperature = 33.35 - 0.53\ wt\% - 0.00052\ SD + 9.68\ SV - 0.353L \\ &R - square\ value = 95.17\% \end{aligned} \quad (3)$$

The wear rate is in mm^3/m, temperature is in °C. The R-square value of the COF, wear rate, and temperature rise is found from the above equations, which can be used to predict the behavior of nanocomposites. The wear rate, COF regression coefficient and temperature rise of the models are 0.8715, 0.9606 and 0.9517 respectively.

From the above regression equations (1)–(3), it is observed that there is a positive load coefficient in the regression equation, which means that as load increases, the COF and wear rate of the MMNCs also increases. This attributes to the fact that, there is increase in the reinforced particles fracture as well as penetrating ability in the steel disc with increase in applied load. Similarly, for the sliding speed (SV), there is positive value in the regression equation of wear rate and temperature rise. It indicates that with a rise in temperature, wear rate of MMNCs increases, while also increasing the sliding speed. This aspect applies to the extension of oxidation and hairline fracture of particles but in case of the COF, it is showing the negative in regression, which means COF decreases with increasing of sliding speed because of solid lubricant film forming on the contact surface. Wt.% reports negative value in the regression equation which indicates that the wear rate, temperature rise and COF of MMNCs decrease with increase of the wt.% of reinforcement content [53].

5. Morphology

The wear test samples were worn surface of novel Al7150-hBN MMNCs as shown in Fig. 12a–i. The morphological studies of wear surface with SEM signify the occurrence of delamination and abrasive wear mechanism in Al7150-hBN MMNCs. Fig. 12a shows the monolithic alloy worn surface at min parameters like applied load, sliding velocity and sliding distance as 10 N, 0.5 m/s, 500 m respectively and disclose the patches of severely damaged areas, as well as deep abrasion grooves due to low speed and the delamination [54], as well as severe wear noticed in the monolithic alloy.

Fig. 12b shows the worn surface of the monolithic alloy at max levels of parameters applied load, sliding velocity and sliding distance as 50 N, 2.5 m/s, 2500 m while reveal many plastic deformation layers and deep grooves due to high friction and hence high temperature, which softens the material, resulting in heavy plastic deformation and oxide layers. Fig. 12a and b shows the parameter effect when it is at a low level and to when it attains max level. Low levels result in more delamination and abrasive wear. Also at max level the material results with heavy plastic deformation.

Fig. 12c shows the worn surface of the 1.5 wt% hBN MMNCs at various levels of parameters like 20 N, 2 m/s, 500 m which in turn reveals the abrasive wear with delamination. Fig. 12d shows the worn surface of 1.5 wt% hBN MMNCs with a load of 50 N, sliding speed of 1 m/s and sliding distance of 2000 m. There is abrasive wear with deeper grooves due to an increase of hBN; the plastic deformation can be restricted and acts as a protective layer, which results in min surface damage. From Fig. 12c and d it can be observed that the increase of parameters (i.e., load from 20 N to 50 N, sliding distance from 500 m to 2000 m) reveals the abrasive wear and delamination. There is more delamination at the min level of parameters (i.e., 20 N, and 500 m) as compared to the max level of parameters (i.e., 50 N, and 2000 m) and deeper grooves than usual.

Fig. 12e shows the worn surface of 2 wt% hBN MMNCs at various levels of parameters (i.e., 50 N, 0.5 m/s, 1000 m) and it reveals wear with more delamination. The debris and oxide layer formation can be observed at a lower speed on the worn surface. Fig. 12f shows the worn surface of 2 wt% hBN MMNCs at various levels of parameters (i.e., 30 N, 2 m/s, 2500 m) which indicates heavy plastic deformation with layer formation. From Fig. 12e and f more delamination and debris can be observed at 50 N, 0.5 m/s, 1000 m MMNCs than 50 N, 0.5 m/s and 1000 m MMNCs combination worn surface.

Fig. 12g–i shows the worn surface of various MMNCs of a constant load 50 N with different parameters at 500X magnification level. These images reveal abrasive wear, number of debris and size of debris when increasing weight percentage of hBN. Fig. 12g shows a monolithic model which reveals heavy plastic deformation as compared to Fig. 12h. Fig. 12i shows high delamination area and more debris.

Table 9
Wear rate Responses for the signal to noise ratios ***'smaller is better'***.

Level	Wt.%	SD (m)	SV (m/s)	Load (N)
1	−11.271	−12.145	−6.744	−5.484
2	−10.372	−12.422	−10.844	−9.709
3	−10.350	−10.469	−11.684	−10.049
4	−11.039	−8.563	−11.560	−12.803
5	−9.556	−8.989	−11.757	−14.544
Delta	1.715	3.859	5.012	9.060
Rank	4th	3rd	2nd	1st

Table 10
COF Responses for the Signal to Noise Ratios ***'smaller is better'***.

Level	Wt.%	SD (m)	SV (m/s)	Load (N)
1	8.322	8.752	5.837	9.633
2	9.032	9.295	6.721	9.140
3	8.719	8.739	9.052	8.722
4	8.968	8.638	10.153	8.614
5	8.892	8.510	12.170	7.825
Delta	0.710	0.785	6.333	1.809
Rank	4th	3rd	1st	2nd

Table 11
Temperature Responses for Signal to Noise Ratios ***'smaller is better'***.

Level	Wt.%	SD (m)	SV (m/s)	Load (N)
1	−33.59	−33.09	−31.81	−32.52
2	−33.45	−33.12	−32.69	−32.88
3	−33.39	−33.72	−33.50	−33.42
4	−33.17	−33.50	−34.63	−33.83
5	−33.66	−33.85	−34.65	−34.63
Delta	0.49	0.76	2.84	2.11
Rank	4th	3rd	1st	2nd

6. Conclusions

The following are some notable implications of the investigations

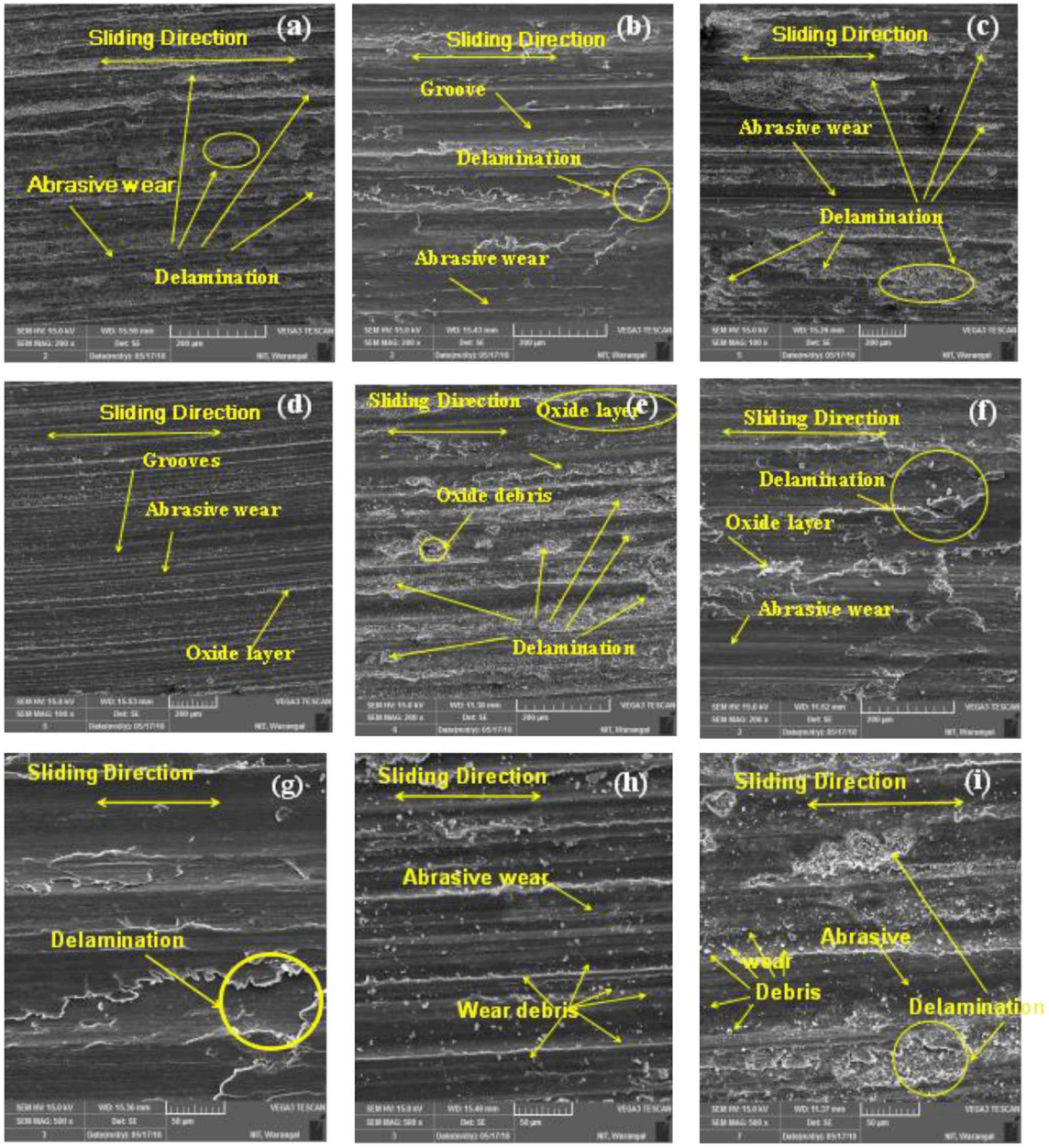

Fig. 12. Worn surface SEM images of AA7150-hBN nanocomposites and monolithic alloy at various combinations such as (a) 0 wt%-10N-0.5 m/s-500 m, (b) 0 wt%-50N-2.5 m/s-2500 m, (c) 1.5 wt%-20N-2m/s-500 m, (d) 1.5 wt%-50N-1 m/s-2000 m, (e) 2 wt%-50N-0.5 m/s-1000 m, (f) 2 wt%-30N-2m/s-2500 m, (g) 0 wt%-50N-2.5 m/s-2500 m, (h) 1.5 wt%-50N-1.5 m/s-2000 m, (i) 2 wt%-50N-0.5 m/s-1000 m.

carried out on Al7150-hBN MMNCs. Al7150-hBN MMNCs containing up to 2 wt% were successfully prepared via liquid metallurgy technique. The density and hardness values were found to increase with increased hBN nano-reinforcement content in the Al7150 up to 1.5 wt% of hBN. The SEM images of Al7150-hBN MMNCs show uniform distribution of nano-particulates in the matrix. The Dry-sliding wear test was conducted to optimize the wear parameters through Taguchi method on Al7150-hBN MMNCs and the following conclusions are drawn from the current investigation.

- ➢ Wear rate, COF and temperature are determined by different factors in order of wt.% of reinforcement, sliding distance, sliding speed and applied load.
- ➢ To determine the influence of dominant parameters on hBN reinforced MMNCs, ANOVA test was conducted and which showed that the wear loss significantly increases with increase of applied load. Similarly, for COF, decreases while temperature increases with increase in sliding speed.
- ➢ The applied load had the greatest influence on statistical and physical properties of MMNCs on dry sliding wear, among all other parameters, such as sliding speed and sliding distance, wt.%.
- ➢ The interactions between SD × Load, wt.% × Load are more influential as compared to other factors interactions on wear rate.
- ➢ The sliding speed had the greatest influence on the COF of nanocomposites, among all other parameters, such as applied load, sliding distance and wt.% of reinforcement.
- ➢ The siding speed had the greatest influence on the temperature of the nanocomposites, among all other parameters, such as the applied load, sliding distance and wt.% of reinforcement particles.

Appendix A. Supplementary data

Supplementary data to this article can be found online at https://doi.org/10.1016/j.compositesb.2019.107136.

References

[1] Madhukar P, Selvaraj N, Rao CSP. Manufacturing of aluminium nano hybrid composites: a state of review. Mater Sci Eng 2016;149:12114. https://doi.org/10.1088/1757-899X/149/1/012114.

[2] Hai Su, Wenli Gao, Hui Zhang, Hongbo Liu, Jian Lu, Zheng Lu. Optimization of stirring parameters through numerical simulation for the preparation of aluminum matrix composite by stir casting process. J. Manuf. Sci. Eng., ASME 2010;132(6):061007. https://doi.org/10.1115/1.4002851.

[3] Veeresh Kumar GB, Rao CSP, Selvaraj N. Studies on mechanical and dry sliding wear of Al6061–SiC composites. Composites Part B 2012;43:1185–91. https://doi.org/10.1016/j.compositesb.2011.08.046.

[4] Chen Baiming, Bi Qinling, Yang Jun, Xia Yanqiu, Jingcheng Hao. Tribological properties of solid lubricants (graphite, h-BN) for Cu-based P/M friction composites. Tribol Int 2008;41:1145–52. https://doi.org/10.1016/j.triboint.2008.02.014.

[5] Yang Y, Li X. Ultrasonic cavitation based nano-manufacturing of bulk aluminum matrix nanocomposites. J. Manuf. Sci. Eng., ASME 2007;129(2):252–5. https://doi.org/10.1115/1.2714583.

[6] Ezatpour HR, Torabi Parizi M, Sajjadi SA. Microstructure and mechanical properties of extruded Al/Al2O3 composites fabricated by stir-casting process. Trans Nonferrous Metals Soc China 2013;23:1262–8. https://doi.org/10.1016/S1003-6326(13)62591-1.

[7] Fadavi Boostania A, Yazdania S, Azari Khosroshahia R, Jiangb ZY, Wei D. A novel graphene-stimulated semi-solid processing to fabricate advanced aluminum matrix nanocomposites. Mater Sci Eng, A 2018;736:316–28. https://doi.org/10.1016/j.msea.2018.09.001.

[8] Shulin Lü, Pan Xiao, Du Yuan, Hu Kun, Wu Shusen. Preparation of Al matrix nanocomposites by diluting the compositegranules containing nano-SiCp under ultrasonic vibaration. J Mater Sci Technol 2018;34:1609–17. https://doi.org/10.1016/j.jmst.2018.01.003.

[9] Xu Tuo, Li Guirong, Xie Menglei, Liu Ming, De Zhang, Zhao Yutao, Chen Gang, Kai Xizhou. Microstructure and mechanical properties of in-situ nano γ-Al2O3p/A356 aluminum matrix composite. J Alloy Comp 2019;787:72e85. https://doi.org/10.1016/j.jallcom.2019.02.045.

[10] Li Jianyu, Zhao Gaozhan, Wu Shusen, Huang Zhiwei, Shulin Lü, Chen Qiang, Li Fei. Preparation of hybrid particulates SiCnp and Mg2Si reinforced Al-Cu matrix Composites. Mater Sci Eng A 2019;751:107–14. https://doi.org/10.1016/j.msea.2019.02.076.

[11] Abu-Warda A, Utrilla MV, Escalera MD, Otero E, López MD. The effect of TiB2 content on the properties of AA6005/TiB2 nanocomposites fabricated by mechanical alloying method. Powder Technol 2018;328:235–44. https://doi.org/10.1016/j.powtec.2018.01.028.

[12] Zhang ZY, Yang R, Li Y, Chen G, Zhao YT, Liu MP. Microstructural evolution and mechanical properties of friction stir processed ZrB2/6061Al nanocomposites. J Alloy Comp 2018;762:312–8. https://doi.org/10.1016/j.jallcom.2018.05.216.

[13] Javad Nasr Isfahani Mohammad, Payami Fereidoun, Asadi Asadabad Mohsen, Asghar Shokri Ali. Investigation of the effect of boron carbide nanoparticles on thestructural, electrical and mechanical properties of Al-B4C. J Alloy Comp 2019;797:1348–58. https://doi.org/10.1016/j.jallcom.2019.05.188.

[14] Popov Vladimir A, Burghammer Manfred, Rosenthal Martin, Kotov Anton. In situ synthesis of TiC nano-reinforcements in aluminum matrix composites during mechanical alloying. Composites Part B 2018;145:57–61. https://doi.org/10.1016/j.compositesb.2018.02.023.

[15] Elkady Omayma A, Abolkassem Shimaa A, Elsayed Ayman H, Hussein Walaa A, Hussein Khalid FA. "Microwave absorbing efficiency of Al matrix composite reinforced with nano-Ni/SiC particles" Results in. Physics 2019;12:687–700. https://doi.org/10.1016/j.rinp.2018.11.095.

[16] Manivannan I, Ranganathan S, Gopalakannan S, Suresh S. Mechanical properties and tribological behavior of Al6061–SiC–Gr self-lubricating hybrid nanocomposites. Trans Indian Inst Met 2018;71:1897–911. https://doi.org/10.1007/s12666-018-1321-0.

[17] Dalmis R, Cuvalci H, Canakci A, Guler O, Celik E. The effect of mechanical milling on graphite–boron carbide hybrid reinforced ZA27 nanocomposites. Arabian J Sci Eng 2018;43:1113–24. https://doi.org/10.1007/s13369-017-2708-7.

[18] Jeyasimman D, Narayanasamy R, Ponalagusamy R, Anandakrishnan V, Kamaraj M. The effects of various reinforcements on dry sliding wear behaviour of AA 6061 nanocomposites. Mater Des 2014;64:783–93. https://doi.org/10.1016/j.matdes.2014.08.039.

[19] Suresh S, Harinath Gowd G, Deva Kumar MLS. Mechanical and wear characterization of Al/Nano-SiC NMMCs by liquid state process. Journal of Bio- and Tribo-Corrosion 2019;5:43–53. https://doi.org/10.1007/s40735-019-0232-x.

[20] Poovazhagan L, Thomas HJ, Selvaraj M. "Microstructure and abrasive wear behavior of copper–boron Carbide nanocomposites" advances in materials and metallurgy. 2019. p. 43–55. https://doi.org/10.1007/978-981-13-1780-4_6.

[21] Roy Debdas, Khobragade Nidhi, Sikdar Koushik, Kumar Binod, Bera Supriya. Mechanical and electrical properties of copper-graphene nanocomposite fabricated by high pressure torsion. J Alloy Comp 2019;776:123–32. https://doi.org/10.1016/j.jallcom.2018.10.139.

[22] Vara Prasad Kaviti R, Jeyasimman D, Parande Gururaj, Gupta Manoj, Narayanasamy R. Investigation on dry sliding wear behavior of Mg/BN nanocomposites. J. Magnesium Alloys 2018;6:263–76. https://doi.org/10.1016/j.jma.2018.05.005.

[23] Zhang Leigang, Luo Xi, Liu Jinling, Leng Yongxiang, An Linan. "Dry sliding wear behavior of Mg-SiC nanocomposites with high volume fractions of reinforcement". Mater Lett 2018;228:112–5. https://doi.org/10.1016/j.matlet.2018.05.114.

[24] Veličković Sandra, Stojanović Blaža, Babić ·Miroslav, Vencl Aleksandar, Bobić Ilija, Vadászné Bognár Gabriella, Vučetić Filip. Parametric optimization of the aluminium nanocomposites wear rate. J Braz Soc Mech Sci Eng 2019;41:19–29. https://doi.org/10.1007/s40430-018-1531-8.

[25] Umanath K, Selavamani ST, Palanikumar K. Friction and wear behaviour of Al 6061 alloy (SiCp+Al203p) hybrid composites. Int. Eng. Sci. Technol. 2011;3:5441–51.

[26] Xiaochun Li, Yong Yang, Xudong Cheng. Ultrasonic-assisted fabrication of metal matrix nanocomposites. J Mater Sci 2004;3(9):3211–2. https://doi.org/10.1023/B:JMSC.0000025862.23609.6f.

[27] Sameezadeh M, Emamy M, Farhangi H. Effects of particulate reinforcement and heat treatment on the hardness and wear properties of AA 2024-MoSi2 nanocomposites. Mater Des 2011;32:2157–64. https://doi.org/10.1016/j.matdes.2010.11.037.

[28] Lian-Yi Chen, Jun-Yang, Peng, Jia-Quan, Xu, Hongseok, Choi, Xiao-Chun Li. Achieving uniform distribution and dispersion of a high percentage of nanoparticles in metal matrix nanocomposites by solidification processing. Scripta Mater 2013;69:634–7. https://doi.org/10.1016/j.scriptamat.2013.07.016.

[29] Veeresh Kumar GB, Rao CSP, Selvaraj N. "Studies on mechanical and dry sliding wear of Al6061–SiC composites". Composites Part B 2012;43:1185–91. https://doi.org/10.1016/j.compositesb.2011.08.046.

[30] Hakimi Chua Abdullah Muhammad Ilman, Bin Abdollah Mohd Fadzli, Tamaldin Noreffendy, Amiruddin Hilmi, Mat Nuri Nur Rashid. Effect of hexagonal boron nitride nanoparticles as an additive on the extreme pressure properties of engine oil. Ind Lubr Tribol 2016;68:441–5. https://doi.org/10.1108/ILT-10-2015-0157.

[31] Shayan Mehrdad, Eghbali Beitallah, Niroumand Behzad. Synthesis of AA2024-(SiO2np+TiO2np) hybrid nanocomposite via stir casting process. Mater Sci Eng A 2019;756:484–91. https://doi.org/10.1016/j.msea.2019.04.089.

[32] Palanikumar K. Application of Taguchi and response surface methodologies for surface roughness in machining Glass fiber reinforced plastics by PCD tooling. Int J Adv Manuf Technol 2008;36(1–2):19–27. https://doi.org/10.1007/s00170-006-0811-0.

[33] Alaneme KK, Ademilua BO, Bodunrin MO. Mechanical properties and corrosion behaviour of aluminium hybrid composites reinforced with Silicon carbide and bamboo leaf Ash. Tribology in Industry 2013;35(1):25-35. http://www.tribology.fink.rs/journals/2013/2013-1/3.pdf.

[34] Baradeswaran A, Elaya Perumal A. Study on mechanical and wear properties of Al 7075/Al2O3/graphite hybrid composites. Composites Part B 2014;56:464–71. https://doi.org/10.1016/j.compositesb.2013.08.013.

[35] Akhlaghi F, Bidaki AZ. Influence of graphite content on the dry sliding and oil impregnated sliding wear behaviour of Al 2024-graphite composites produced by in situ powder metallurgy method. Wear 2009;266(1/2):37–45. https://doi.org/10.1016/j.wear.2008.05.013.

[36] Jerzy Myalski, Andrzej Posmyk. Processing of sliding hybrid composites with aluminium alloy matrix containing solid lubricants. Mater Manuf Process 2015. https://doi.org/10.1080/10426914.2015.1127940.

[37] Ravindran P, Manisekar K, Narayanasamy R, Narayanasamy P. Tribological behaviour of powder metallurgy-processed aluminium hybrid composites with the addition of graphite solid lubricant. Ceram Int 2013;39:1169–82. https://doi.org/10.1016/j.ceramint.2012.07.041.

[38] Chi H, Jianga L, Chen G, Kang P, Lin X, Wu G. Dry sliding friction and wear behavior of (TiB2 + h-BN)/2024Al composites. Mater Des 2015;87:960–8. https://doi.org/10.1016/j.matdes.2015.08.088.

[39] Kumar M, Megalingam Murugan A, Baskaran V, Hanumanth Ramj KS. Effect of sliding distance on dry sliding tribological behaviour of Aluminium Hybrid Metal Matrix Composite (AlHMMC): an alternate for automobile brake rotor – a Grey Relational approach. IMech, SAGE; 2015. https://doi.org/10.1177/1350650115602724.

[40] Baradeswaran A, Elaya Perumal A, Franklin Issac R. A Statistical analysis of optimization of wear behaviour of Al-Al2O3 composites using Taguchi technique. Proced. Eng. 2013;64:973–82. https://doi.org/10.1016/j.proeng.2013.09.174.

[41] Alidokht SA, Abdollah-zadeh A, Assadi H. Effect of applied load on the dry sliding wear behaviour and the subsurface deformation on hybrid metal matrix composite. Wear 2013;305:291–8. https://doi.org/10.1016/j.wear.2012.11.043.

[42] Veeresh Kumar GB, Pramod R, Gouda PS, Rao CSP. Effect of tungsten carbide reinforcement on the aluminium 6061 alloy. J Test Eval 2017:1–32. https://doi.org/10.1520/JTE20170545.

[43] Kiran TS, Prasanna Kumar M, Basavarajappa S, Viswanatha BM. Dry sliding wear behavior of heat treated hybrid metal matrix composite using Taguchi techniques. Mater Des 2014;63:294–304. https://doi.org/10.1016/j.matdes.2014.06.007.

[44] Baradeswaran A, Vettivel SC, Elaya Perumal A, Selvakumar N, Franklin Issac R. Experimental investigation on mechanical behaviour, modelling and optimization of wear parameters of B4C and graphite reinforced aluminium hybrid composites. Mater Des 2014;63:620–32. https://doi.org/10.1016/j.matdes.2014.06.054.

[45] Kumar R, Dhiman S. A study of sliding wear behaviors of Al-7075 alloy and Al-7075 hybrid composite by response surface methodology analysis. J. Mater Des. 2013;50:351–9. https://doi.org/10.1016/j.matdes.2013.02.038.

[46] Murphy S, Savaskan T. Comparative wear behavior of Zn–Al-based alloys in an automotive engine application. Wear 1984;98:151–61. https://doi.org/10.1016/0043-1648(84)90224-2.
[47] Savaskan T, Murphy S. Mechanical properties and lubricated wear of Zn–25Al-based alloys. Wear 1987;116:211–24. https://doi.org/10.1016/0043-1648(87)90234-1.
[48] Jaswinder SINGH. Fabrication characteristics and tribological behavior of Al/SiC/Gr hybrid aluminum matrix composites: a review. Friction 2016;4:191. https://doi.org/10.1007/s40544-016-0116-8.
[49] Uvaraja VC, Natarajan N, Rajendran I, Sivakumar K. Tribological behavior of novel hybrid composite materials using Taguchi technique. Journal of Tribology, ASME 2013;135(2):021101–12. https://doi.org/10.1115/1.4023147.
[50] Baradeswaran A, Elaya Perumal Department A. Wear and mechanical characteristics of Al 7075/graphite composites. Compos. Part B 2014;56:472–6. https://doi.org/10.1016/j.compositesb.2013.08.073.
[51] Vettivel SC, Selvakumar N, Narayanasamy R, Leema N. Numerical modelling, prediction of Cu–W nano powder composite in drysliding wear condition using response surface methodology. Mater Des 2013;50:977–96. 2013, https://doi.org/10.1016/j.matdes.2013.03.072.
[52] Bodunrin MO, Alaneme KK, Chown LH. Aluminium matrix hybrid composites: a review of reinforcement philosophies; mechanical, corrosion and tribological characteristics. J. Mater. Res. Technol 2015;4(4):434–45. https://doi.org/10.1016/j.jmrt.2015.05.003.
[53] Vettivel SC, Selvakumar N, Leema N, Lenin A Haiter. Electrical resistivity, wear map and modelling of extruded tungsten reinforced copper composite. Mater Des 2014;56:977–96. https://doi.org/10.1016/j.matdes.2013.11.070.
[54] Basavarajappa S, Chandramohan G, Mukund K, Ashwin M, Prabu M. Dry sliding wear behavior of Al 2219/SiCp-Gr hybrid metal matrix composites. JMEP 2006;15:668–74. https://doi.org/10.1361/105994906X150803.